Resonant x-ray scattering observation of transitional subphases during the electric-field-induced phase transition in a mixture of Se-containing chiral smectic liquid crystals

Atsuo Iida, Yoichi Takanishi, Atsuo Fukuda, and Jagdish K. Vij

Phys. Rev. E **97**, 062702 — Published 12 June 2018

DOI: 10.1103/PhysRevE.97.062702

Resonant X-ray scattering observation of transitional subphases during the electric-field-induced phase transition in a mixture of Se-containing chiral smectic liquid crystals

Atsuo Iida[1)], Yoichi Takanishi[2)], Atsuo Fukuda[3)], and Jagdish K. Vij[3)]

1) Photon Factory, Institute of Materials Structure Science, High Energy Accelerator Research Organization, 1-1 Oho Tsukuba, Ibaraki 305-0801, Japan
2) Department of Physics, Faculty of Science, Kyoto University, Kitashirakawa-oiwake, Sakyou-ku Kyoto 606-8502, Japan
3) Department of Electronic and Electrical Engineering, Trinity College, The University of Dublin, Dublin 2, Ireland

Abstract

Using resonant X-ray scattering techniques, transitional subphases during the electric-field-induced phase transition of a mixture of Se-containing chiral liquid crystals, 80% AS657 and 20% AS620, in a planar-aligned cell geometry were investigated, where the prototypical phase sequence SmC_A^*-SmC_γ^*-AF- SmC^* was observed; the transitional subphases were formed during the transition from the three-layer periodicity phase to the ferroelectric phase. In the lower temperature range where the three-layer SmCγ* phase appeared under the low electric field, nine-layer and six-layer subphases, and "streak" pattern appeared in sequence after the transition from the SmCγ* phase with increasing applied electric field; the ferroelectric phase was realized. In the higher temperature range where the four-layer AF phase appeared under a low electric field, the AF phase changed to a three-layer phase at the medium electric field. The twelve-, nine-, and six-layer subphases subsequently appeared in sequence, and finally the ferroelectric phase was

generated with increasing electric field. The molecular arrangements of the field-induced subphases, especially the newly-found nine-layer periodicity phase, was analyzed. The successive field-induced phase transition of the present results was compared with that of our previous results for pure Se-containing and Br-containing liquid crystals and the relation to the three-layer ferrielectric phase was discussed.

I. Introduction

Various subphases of chiral smectic-*C* liquid crystals (LCs), which are characterized by an azimuthal arrangement of molecular orientations among the layers, were discovered between the lower-temperature antiferroelectric (SmC_A^*) and higher-temperature ferroelectric (SmC^*) phases [1–3]. The long-range interlayer interaction, which is the origin of these subphases, has attracted much attention both experimentally [4–8] and theoretically [9–13]. In the SmC^* and SmC_A^* phases, the molecules in adjacent layers are oriented in a synclinic and anticlinic manner, respectively [1, 4], while the ferrielectric (SmC_γ^*) and antiferroelectric (AF) subphases, which lie between the SmC^* and SmC_A^* phases, have three- and four-layer periodic structures, respectively [5–8]. In the assignment and characterization of these chiral smectic-*C* subphases, the resonant x-ray scattering (RXS) technique has played a crucial role [5–8, 14–17] because it provides the unique technique to determine the layer periodicity and its parameters. In addition to the phases with two-, three-, and four-layer periodicity, two types of smectic phases with a six-layer periodic structure have been experimentally observed by Huang *et al.* [14–16] and Takanishi *et al.* [17] in different LCs. Furthermore, novel subphases with seven-, eight- and ten-layer periodic structures were reported for Br-containing LCs and Se-containing LC mixtures based on RXS analysis [18, 19].

Not only the temperature-induced phase transition but also an electric-field-induced phase transition in these chiral smectic LCs from low-field subphases to the high-field SmC^* phase has

been extensively studied [1, 20–25]. Among them, RXS studies have directly revealed a sequential field-induced phase transition from the AF phase at low field, the SmC^*_γ phase at medium field, and the SmC^* phase at high field using samples with a device geometry (planar aligned cell structure) [26–28]. Recently, in a Br-containing chiral LC, a field-induced transitional subphase with twelve-layer periodicity was found between the SmC^*_γ phase and the SmC^* phase by microbeam RXS analysis with the device geometry [29]. More recently, using the same technique, field-induced transitional subphases with *n*-layer (*n* = 5 to 8, depending on the temperature) periodicity were revealed in a pure Se-containing LC [30]. Some of these transitional subphases showed unique characteristics, which have not yet been experimentally or theoretically reported and been revealed by the combination of the microbeam RXS, the sample of the device geometry and the 2D detector. It is noted, however, that the observed transitional subphases were different for the two Br- and Se-containing samples, though temperature-electric field phase diagrams of both samples were similar except for the high-temperature SmC^*_α phase in the pure Se-containing LC. In order to further investigate a variety of field-induced transitional subphases, in this report, we use a Se-containing mixture LC sample that shows a phase sequence SmC^*_A - SmC^*_γ - AF - SmC^* with increasing temperature; i.e. the typical case of the frustration between the SmC^*_A and SmC^* phases [19].

II. Experimental

A Se-containing LC mixture sample comprising 80% AS657 and 20% AS620 [7, 19, 23, 31, 32] (see Fig. 1) was used in the experiment. AS657 and AS620 were purchased from Kingston Chemicals Ltd., University of Hull, Hull, U.K. The sample had a typical phase sequence of SmC_A^* (85.8 °C) SmC_γ^* (87.7 °C) AF (89.8 °C) SmC^* with heating [19]. The phase transition temperatures given in parentheses were obtained during X-ray experiments.

The experimental conditions and procedures used herein are the same as those in previous studies [29, 30], and only a brief summary is presented here. The sample was inserted into a 25-μm-thick sandwich cell having two 80-μm-thick glass plates for substrates coated with indium tin oxide as electrodes. One side of the glass plate was coated with polyimide and was rubbed. The sample cell was mounted on a compact heater. To obtain a uniform layer structure, a square-wave electric field (±95 V maximum) was applied around 80 °C, and the sample was then heated to the temperature of the target phase. The samples were examined in the lower temperature range of the SmC_γ^* (86.3 °C and 86.6 °C) phase and the higher temperature range of the AF (88.0 °C) phase. The applied alternating electric field was a square waveform of 100 Hz.

RXS experiments were performed on the 4A beamline at the Photon Factory (Japan). A monochromatic X-ray microprobe with a 5 x 5 μm^2 square beam was used. The incident X-ray energy was set to the absorption edge of Se (12.65 keV). The layer normal of the homogeneously

aligned cell was approximately horizontal, and a vertical rotation axis was adopted. A pixel array X-ray detector (Pilatus-100K, DECTRIS) was located at 100 cm through 117 cm from the sample. A polarizing optical microscope was used to monitor the optical response of the sample during the measurement. The temperature stability of the sample was better than ±0.03 °C during the measurement.

At each applied electric field, the X-ray incident angle was adjusted to the RXS satellite peak position of interest by rotating the sample (ω-intensity profile), and then intensity measurement was carried out without sample rotation using the two-dimensional (2D) detector. The q/q_0 intensity distribution in the radial direction, where q is the scattering vector and $q_0 = 2\pi/d$ (d is the smectic layer spacing), was extracted from the recorded 2D pattern. The first-order Bragg peak position in the 2D pattern was approximated as q_0, and the obtained intensity distribution was analyzed semiquantitatively based on the RXS theory [33, 34]. The RXS reflections appearing near the forward scattering direction ($q/q_0 < 1$) were measured to attain a reasonable detection efficiency, while a direct beam stopper blocked scattered X-rays in the small q region.

During the course of our studies of the transitional subphases [29, 30], we adopted a combination of samples of the device geometry, the microbeam RXS technique and the 2D detector. This technique has three main advantages: 1) the homogeneous electric field application is assured by the conventional device geometry, 2) controlled and uniform temperature and electric fields are

guaranteed in the small sample volume defined by X-ray microbeams together with the *in-situ* polarizing microscope observation, and 3) the wide q-range in the reciprocal space can be studies simultaneously, so that the long-periodicity phases and other characteristics (e.g. “streak pattern”, satellite peaks at incommensurate positions and so on [30]) are identified.

III. Results

At 86.3 °C (0.5 °C above the SmC_A^*-to-SmC_γ^* phase transition temperature), RXS analysis indicated the formation of a three-layer periodic structure (C_{3p} phase hereafter) below ±45.0 V [Fig. 2(a)]. At ±45.2 V and ±45.6 V, a weak thread-like phase boundary moved across the field of view [Fig. 3(a)]. At the same time, a peak appeared at q/q_0 = 0.22 (2/9) (Fig. 2(b) and (c)), and very weak humps were discernible at q/q_0 = 0.44 (4/9) and 0.56 (5/9) in addition to the strong peaks at q/q_0 = 1/3 and 2/3 [Fig. 2(c)]. The peaks at ±45.6 V seemed to correspond to the nine-layer periodic structure (C_{9p} phase hereafter), though the peaks at q/q_0 = 7/9 and 8/9 could hardly be observed. At ±45.2 V, the C_{3p} and C_{9p} structures coexisted. At ±47.0 V, the peaks related to the C_{9p} structure became very weak and, in addition to the q/q_0 = 1/3 and 2/3 peaks, peaks at q/q_0 = 0.5 (1/2) and 0.17 (1/6, very close to the direct beam stopper) and weak peaks at q/q_0 = 0.83 (= 5/6) appeared [Fig. 2(d)]. These peaks correspond to a six-layer periodic structure (C_{6p} phase hereafter). At a high applied voltage (±49.0 V), the peaks became weak and broad [Fig. 2(f)]. At ±52.0 V, the peaks disappeared and a streak pattern ("streak" hereafter), i.e., a diffraction profile with no conspicuous reflection peaks [29], remained [Fig. 2(f)]. At ±54.5 V, the SmC^* (ferroelectric) phase was detected at the measurement point [Fig. 3(b)].

The measurement was also carried out at 86.6 °C, i.e., 0.3 °C above the previous temperature, and the SmC_γ^* phase was still observed without the electric field. Nearly the same field-induced

phase transition occurred as for the previous temperature (86.3 °C), though the transition voltages were slightly different: C_{3p} (±40.8 V) C_{9p} (±42.8 V) C_{6p} (±47.5 V) "streak" (±51.6 V) SmC^*.

At 88.0 °C (0.3 °C above the SmC^*_γ-to-AF phase transition temperature), the RXS pattern showed reflections at q/q_o = 1/4 and 3/4 up to ±21.0 V [Fig. 4(a)], which was a typical diffraction profile for the four-layer periodicity (AF) phase (C_{4p1} phase hereafter). The polarizing microscope image showed a weak stripe texture running parallel to the smectic layer [Fig. 5(a)]. At ±21.5 V, the stripe texture disappeared [Fig. 5(b)], and peaks corresponding to the C_{3p} phase appeared at q/q_o = 1/3 and 2/3, as shown in Fig. 4(b). These remained unchanged up to ±30.0 V. At ±30.4 V [Fig. 4(c)], in addition to the peaks of the C_{3p} phase, a peak appeared at q/q_o = 1/4. Then, at ±30.6 V [Fig. 4(d)], weak peaks appeared at q/q_o = 0.42 (5/12), 0.58 (7/12), and 0.75 (9/12). At the same time, a very weak stripe texture appeared in the sample [Fig. 5(c)]. It appears that the 12-layer (C_{12p} hereafter) phase was formed at this applied voltage, while no peaks were observed at q/q_o = 6/12, 10/12, and 11/12 (if present, the 1/12 reflection was blocked by the direct beam stopper).

At a slightly higher voltage of ±31.2 V [Fig. 4(e)], in addition to the peaks at q/q_o = 1/3 and 2/3, peaks appeared at q/q_o = 0.22 (2/9), 0.44 (4/9), 0.56 (5/9), and 0.77 (7/9). These peak positions correspond to those expected for the C_{9p} phase, though the peaks at q/q_o = 1/9 and 8/9 were difficult to observe. At ±32.6 V [Fig. 4(f)], the C_{9p} phase was still partially present given that peaks were clearly observed at q/q_o = 0.22, 0.33, 0.66, and 0.78, though the peaks at q/q_o = 0.4−0.6 were too

weak and broad to assign a specific q-value. At ±33.7 V [Fig. 4(g)], the peaks appeared to correspond to the C_{6p} phase, though they became slightly broad. At this stage, the stripe texture gradually became clearer [Fig. 5(d)]. The peaks became broad and weak at ±36.0 V (thick solid line in Fig. 4(h)), and the "streak" pattern appeared at ±40.0 V (thin solid line (blue) in Fig. 4(h)) prior to the transformation to the SmC^* phase at ±42.0 V. In summary, the transitional subphases that appeared at this temperature were as follows: C_{4p1} (±21.5 V) C_{3p} (±30.6 V) C_{12p} (±31.2 V) C_{9p} (±33.7 V) C_{6p} (±40.0 V) "streak" (±42.0 V) SmC^*.

At higher temperatures where the AF phase was generated without an applied electric field, the RXS diffraction profile was often complicated, and the reproducibility of the measurements was poor. Although the phases seemed to reflect the sample history, these experimental conditions required for the good repeatability have not been clarified. In the present studies, therefore, only the transitional subphases that could be reproducibly formed at lower temperatures are reported and discussed.

IV. Discussions

The C_{6p}, C_{9p}, and C_{12p} transitional subphases were observed during the field-induced transition from the C_{3p} phase to the SmC^* phase. The present sample was already used to study the subphases appearing just below and above SmC^*_γ phase at the low applied electric field by the electric-field-induced birefringence and micro-RXS techniques [19]. The field-induced phase transition from the SmC^*_γ (C_{3p}) to SmC^* phases is clearly observed in their E-T diagram as a narrow region (line A-B in Fig2 (a) shown in ref. [19]). However, the detail of the field-induced phase transition is not clear at high fields.

First, the molecular configurations of these subphases are discussed. At 86.3 °C and around ±45.6 V [Fig. 2(c)], and at 88.0 °C and around ±31.2 V [Fig. 4(e)], the nine-layer periodic structure appeared to be formed because the 4/9 and 5/9 reflections were unique to the nine-layer periodicity. The intensities of the peaks at q/q_o = 1/3 and 2/3 were stronger than those of the other peaks, even though the experimental condition was optimized for the q/q_o = 1/3 peak. The Ising (flat) molecular arrangements are discussed as a starting molecular configuration. Though the number of all possible combinations of the directions of the director of each layer are quite large (2^9), that of the independent molecular arrangements was found to be limited to 21 configurations (except for the trivial configurations such as three- and single-layer) as shown in Table 1, where $\{\cdots\}$ represents the molecular configuration in a unit cell, and “R” and “L” indicate the smectic layer with directors

tilted to the right and left, respectively. Table 1 also shows the corresponding calculated squares of the structure factor (RXS peak intensities without geometrical factors, Int-SF hereafter) of each satellite peak. It is noted that Int-SF is equal for the peaks at $q/q_o = m/9$ and $(9 - m)/9$. Among them, five configurations have the strong 3 (6) / 9 reflections (Nos. 5, 14, 17, 19, and 20), and furthermore only one molecular configuration (No.5) gives the RXS peak intensity ratio similar to the experimental result, namely, {RRRRRLRRL} (or $\{R^3 (R^2L)^2\}$). Other four configurations give too strong (No.17 and 20) and too weak (No.14 and 19) 4 (5) / 9 reflections. Although the {RRLRRLRLL} ($\{(R^2L)^2 RL^2\}$) configuration (No.19) has a rather weak 4 (5) / 9 reflection compared to the experimental result, two structures (No.5 and 19) can be the candidates for the newly-found nine-layer structure within the present experimental precision.

For assessing the configuration under the electric field, the value $q_E = |[R] - [L]| / ([R] + [L])$ is sometimes effective, where $[R]$ and $[L]$ are the number of "R" and "L" layers in a unit cell [25]. A higher applied voltage is expected to produce a molecular arrangement having a larger q_E. In the present case, because the C_{3p} configuration (q_E =1/3) is generated at a lower electric field for the lower temperature SmC^*_γ (86.3 °C and 86.6 °C) phase, the $\{R^3 (R^2L)^2\}$ (q_E = 5/9) configuration is more probable than the $\{(R^2L)^2 RL^2\}$ (q_E = 1/9) configuration.

The clock model is clearly excluded in the present case because it produces a diffraction profile in which only the 1/9 and 8/9 reflections are strong. For the distorted clock model, the introduction

of the distortion angle (δ) into the Ising model is a simple procedure, where δ is defined as the smallest rotation angle of the director between two successive layers. Although the distortion angle affects the Int-SF ratio, the correction was relatively small for the $\{R^3 (R^2L)^2\}$ structure with a small δ value (for example, less than ca. 50°). The distorted clock model of the C_{9p} structure, however, should be discussed in more detail because many types of distorted clock configurations can be considered for the C_{9p} structure. The high precision experiment is needed to precisely determine the molecular configuration and parameters, such as the helical pitch and the distortion angle. Hence, the more detailed discussions and analyses are necessary to determine the conclusive molecular arrangement in this transitional subphase.

As far as the authors know, for the C_{9p} structure, no experimental RXS data has been documented, whereas three molecular configurations were proposed based on theoretical consideration [10, 35, 36]. The nine-layer periodic phase without an electric field was discussed by Emelyanenko and Osipov [10], in which the distorted clock version of the $\{R (RL)^4\}$ configuration was proposed. Their configuration, however, produces a considerably different RXS diffraction pattern from the present experimental result as shown in Table 1 (no. 21), where only the two peaks at q/q_o = 4/9 and 5/9 are strong. The other two calculations [35, 36] discussed the possibility of the $\{R^3 (R^2L)^2\}$ configuration, i.e. the same as the present one. The configuration model "$q_E n$ = 3" proposed by Chandani et al. [35] under an electric field is the same as the present one, but those

authors concluded that the "$q_E n$ = 3" model was difficult to be stabilized from the free-energy density point of view. Furthermore, the sequential phase transition, i.e. from nine-layer to six-layer structure, was not explained by their calculation. The "q_T = 5/9" model developed by Emelyanenko [36] under an electric field is also the same as the present configuration; however, the "q_T = 5/9" model seems to appear in the wider range of electric fields than those observed herein and we have not observed subphases which were shown in his E-T diagram. Though these two calculated configurations proposed the same molecular arrangement as the present results, they are still insufficient to fully explain the present results.

Satellite peaks at $q/q_o = m/6$ (m =2–5) were observed at 86.3 °C at around ±47.0 V [Fig. 2(d)], and at 88.0 °C at around ±33.7 V [Fig. 4(g)]. The three experimentally obtained C_{6p} structures were the $\{R^3L^3\}$ ($\delta = 27°$) [14, 16] and the $\{R^4L^2\}$ [17, 37] configurations without an electric field, and the $\{R^5L\}$ configuration under an electric field [30]. Other possible C_{6p} configurations have also been discussed [15, 30]. Among them, the $\{R^5L\}$ structure (with a small distortion angle, if any) seems to be a suitable candidate for the present C_{6p} configuration because it produces a nearly equal satellite peak intensity, as discussed in a previous paper [30].

The multiple peaks at 88.0 °C at around ±30.6 V [Fig. 4(d)] appear to be related to the C_{12p} structure, which was previously reported for a Br-containing LC [29] and was assigned to the $\{R^6(R^2L)^2\}$ configuration, where the calculated Int-SF of the satellite peak for $q/q_o = m/12$ (m = 1–6) is

$<<8 : 0 : 8 : 16 : 8 : 0>>_{Int}$, where $<<\ldots..>>_{Int}$ represents the relative Int-SF for each peak . It is noted again that Int-SF is equal for the peaks at $q/q_o = m/12$ and $(12 - m)/12$ (m = 1–5). The C_{12p} structure in the present experiment may result from the same $\{R^6 (R^2L)^2\}$ configuration because the present satellite peak intensity ratio is similar to the previous one, i.e., the satellite intensities at $q/q_o = m/12$ (m = 4 and 8) are strong, those at $q/q_o = m/12$ (m = 3, 5, 7, 9) are relatively weak, and the satellite at q/q_o = 1/2 (6/12) is absent or very weak (the very weak intensities peaks at q/q_o = 11/12 are tentatively proposed to result mainly from the geometrical factor). Owing to the semiquantitative nature of the present analysis and considering the large number of possible molecular configurations of the C_{12p} structure and their modifications to the distorted clock model, more complicated distorted C_{12p} structures cannot be excluded. A distorted clock model of the 12-layer periodicity structure was recently proposed [35]; however, no appreciable intensity change was expected owing to the small distortion angles.

A single phase is assumed throughout the above analysis. However, the coexistence of some phases cannot be ignored. For the C_{12p} structures, for example, the peaks at $q/q_o = m/12$ (m = 4, 8) and $m/12$ (m = 3, 6, 9) might be assigned to the C_{3p} (or C_{6p}) and C_{4p1} structures, respectively, whereas the peaks at q/q_o = 0.41 and 0.58 should still be assigned to those at q/q_o = 5/12 and 7/12 of the C_{12p} configuration, respectively. Furthermore, a mixture of several C_{12p} configurations cannot be ignored in principle. A similar argument can be also raised for the C_{9p} structure. When the phase

mixture is taken into account, it is difficult to discuss the molecular configuration in the present experiment. Experimentally, however, the transitional subphases are reproducible and relatively stable; therefore, they are considered to be a single phase except for the apparent transient phases caused by the gradual movement of the phase boundary during the measurement [for example, see Fig. 2(b)].

The field-induced transitional subphases differed for the three samples evaluated using the microbeam RXS technique, though the major temperature-electric field phase diagrams were similar except for the higher-temperature phase, which is SmC* phase for the present Se-mixture sample and Br-containing sample [29] and the SmC^{*}_{α} phase for the previous pure-Se sample [30]. In the present results, the field-induced transitions at lower temperatures (86.3 °C and 86.6 °C) occurred from low to high fields as C_{3p} => C_{9p} => C_{6p} => "streak" => SmC*. However, for the pure Se-containing [30] and the Br-containing [29] LCs, the C_{3p} => C_{6p} => "streak" => SmC* and C_{3p} => C_{12p} => "streak" => SmC* transitions were respectively observed. For both cases, the field-induced transition seems to occur on the basis of a three-layer block; the RRL block (and its equivalent configurations, RLR and LRR) changes to an RRR block by simply flipping the director of one molecule. The C_{12p} $\{R^6\ (R^2L)^2\}$ (q_E =2/3) structure changes two blocks in every four blocks, whereas the C_{9p} $\{R^3\ (R^2L)^2\}$ (q_E =5/9) and C_{6p} $\{R^3\ R^2L\}$ (q_E =2/3) structures are achieved by changing one block in every three and two blocks, respectively.

The field-induced transitions at higher temperature (88.0 °C) are more complicated. With increasing an electric field, the following transition occurred: (C_{4p}=>) C_{3p}=> C_{12p} => C_{9p} => C_{6p} => "streak" => SmC* in the present sample, while the (C_{4p}=>) C_{3p}=> "peak shift (3/4)" => C_{vp} (v = 5–8) => "peak shift" => "streak" => SmC* transition occurred in the pure Se-containing sample [30]. The transition in the present sample appears to be similar to that at lower temperatures, i.e., the transition is based on a three-layer block, whereas that in the pure Se-containing sample involves a simple increase in periodicity. Furthermore, the present C_{12p} structure of the $\{R^6 (R^2L)^2\}$ (q_E = 2/3) configuration is difficult to understand because the phase sequence C_{3p} (q_E = 1/3) => C_{12p} (q_E = 2/3) => C_{9p} (q_E = 5/9) => C_{6p} (q_E = 2/3) does not agree with the conventional criterion in which the q_E value increases with the applied voltage; another configuration of $\{R^3 (R^2 L)^3\}$ (q_E = 1/2) might be assigned to the observed C_{12p} structure, although the calculated Int-SF $<<4 : 4 : 4 : 36 : 4 : 4>>_{Int}$ for the Ising (flat) model is less suitable for explaining the observed almost zero intensity at q/q_o = 1/2 (6/12). At higher temperatures, where the AF phase appeared under the low electric field, the observed phase transition of the mixture and pure Se-containing samples from the C_{3p} to SmC* phase is quite different, whereas that from the AF to C_{3p} phase is the same. It might be possible to speculate that the C_{3p} structure have a delicate fine substructure that depends on the mixing ratio of binary samples as well as the temperature and the electric field. Comprehensive experimental studies are needed to clarify the transitional subphases at high temperatures.

V. Conclusions

We have observed the transitional subphases appearing during the successive electric field-induced phase transition from three-layer SmCγ* phase to the high-field SmC^* phase using the micro RXS technique in a mixture of Se-containing chiral liquid crystals. In the lower temperature range, the three-layer SmCγ* phase changed to the nine-layer and six-layer subphases in sequence with increasing applied electric field. In the higher temperature range where the four-layer AF phase appeared under a low electric field, above the three-layer phase at the medium electric field, the twelve-, nine-, and six-layer subphases appeared in sequence below the SmC^* phase was generated. The molecular arrangements of the nine-layer periodicity phase which has not been reported so far was analyzed by the RXS theory and $\{R^3 (R^2L)^2\}$ configuration was found to be the most provable molecular arrangement among 21 possible configurations for the nine-layer phase. There is no theoretical model which fully explain the present field-induced nine-layer subphase. On the other hand, the six- and twelve-layer periodicity structures were the same as our previous results. From the present results, together with our previous experimental results for pure Se-containing and Br-containing liquid crystals, the typical field-induced transitional subphases appearing between the SmCγ*and SmC^* phases were the long-periodicity modification of the three-layer configuration.

Acknowledgements

The authors would like to thank Ms. Y. Ohtsuka and the staff of the Photon Factory for their help during the experiments. This work was carried out under the approval of the Photon Factory Advisory Committee (Proposal Nos. 2014G638 and 2016G604). This work was partly supported by a Grant-In-Aid for Scientific Research on Priority Area (A) (23246007) of the Ministry of Education, Culture, Sports, Science and Technology. Work of the Dublin group was supported by the Ireland-Japan International Strategic Cooperation Award and partly by 13/US/I2866 from the Science Foundation of Ireland as a US–Ireland Research and Development Partnership program administered jointly with the United States National Science Foundation under grant number NSF-DMR-1410649.

References

[1] A. Fukuda, Y. Takanishi, T. Isozaki, K. Ishikawa, and H. Takezoe, J. Mater. Chem.**4**, 997 (1994).

[2] S. T.Lagerwall, *Ferroelectric and Antiferroelectric Liquid Crystals* (Wiley, Weinheim, 1999).

[3] H. Takezoe, E. Gorecka and M. Čepič, Rev. Mod. Phys., **82**, 897 (2010).

[4] A. D. L. Chandani, E. Gorecka, Y. Ouchi, H. Takezoe, and A. Fukuda, Jpn. J. Appl. Phys. **28**, L1265 (1989).

[5] P. Mach, R. Pindak, A. M. Levelut, P. Barois, H. T. Nguyen, C. C. Huang, and L. Furenlid, Phys. Rev. Lett. **81**, 1015 (1998).

[6] A. Cady, J. A. Pitney, R. Pindak, L. S. Matkin, S. J. Watson, H. F. Gleeson, P. Cluzeau, P. Barois, A.-M. Levelut, W. Caliebe, J. W. Goodby, M. Hird, and C. C. Huang, Phys. Rev.E **64**, 050702 (2001)

[7] L. S. Hirst, S. J. Watson, H. F. Gleeson, P. Cluzeau, P. Barois, R. Pindak, J. Pitney, A. Cady, P. M. Johnson, C. C. Huang, A. M. Levelut, G. Srajer, J. Pollmann, W. Caliebe, A. Seed, M. R. Herbert, J. W. Goodby, and M. Hird, Phys. Rev. E **65**, 041705 (2002).

[8] N. W. Roberts, S. Jaradat, L. S. Hirst, M. S. Thurlow, Y. Wang, S. T. Wang, Z. Q. Liu, C. C. Huang, J. Bai, R. Pindak and H. F. Gleeson, Europhys. Lett. **72**, 976 (2005).

[9] M. A. Osipov, A. Fukuda, and H. Hakoi, Mol. Cryst. Liq. Cryst. **402**, 9 (2003).

[10] A. V. Emelyanenko and M. A. Osipov, Phys. Rev. E **68**, 051703 (2003).

[11] P. V. Dolganov, V. M. Zhilin,V. K. Dolganov and E. I. Kats, Phys. Rev. E **67**, 041716 (2003).

[12] M. B. Hamaneh and P. L. Taylor, Phys. Rev. Lett. **93**, 167801 (2004).

[13] P. V. Dolganov, V. M. Zhilin, and E. I. Kats, *J. Exp. Theor. Phys.*, **115**, 1140 (2012).

[14] S. Wang, L. D. Pan, R. Pindak, Z. Q. Liu, H. T. Nguyen, and C. C. Huang, Phys. Rev. Lett. **104**, 027801 (2010).

[15] L. D. Pan, R. Pindak and C. C. Huang, Phys. Rev. E **89**, 022501 (2014).

[16] C. C. Huang, Shun Wang, LiDong Pan, Z. Q. Liu, B. K. McCoy, Y. Sasaki, K. Ema, P. Barois and R. Pindak, Liquid Crystal Reviews **3**, 58 (2015).

[17] Y. Takanishi, I. Nishiyama, J. Yamamoto, Y. Ohtsuka and A. Iida, Phys. Rev. E **87**, 050503(R) (2013).

[18] Y. Takanishi, Y. Ohtsuka, Y. Takahashi, S. Kang and A. Iida, EPL, **109**, 56003 (2015)

[19] Z. Feng, A. D. L. Chandani, A. Fukuda, J. K. Vij, K. Ishikawa, A. Iida, and Y. Takanishi, Phys. Rev. E **96**, 012701 (2017)

[20] Yu. P. Panarin, O. Kalinovskaya, J. K. Vij and J. W. Goodby, Phys. Rev.E **55**, 4345 (1997).

[21] K. Hiraoka, Y. Takanishi, K. Skarp, H. Takezoe, and A. Fukuda, Jpn. J. Appl. Phys. **30**, L1819 (1991).

[22] N. M. Shtykov, J. K. Vij, R. A. Lewis, M. Hird, and J. W. Goodby, Phys. Rev. E **62**, 2279 (2000).

[23] L. S. Matkin, S. T. Watson, H. F. Gleeson, R. Pindak, J. Pitney, P. M. Johnson, C. C. Huang, P.

Barois, A. M. Levelut, G. Srajer, J. Pollmann, J. W. Goodby and M. Hird, Phys. Rev. E **64**, 021705 (2001).

[24] A. D. L. Chandani, N. M. Shtykov, V. P. Panov, A. V. Emelyanenko, A. Fukuda, and J. K. Vij, Phys. Rev. E **72**, 041705 (2005).

[25] K. L. Sandhya, A. D. L. Chandani, A. Fukuda, S. Kumar, and J. K. Vij, Phys. Rev. E **87**, 062506 (2013).

[26]S. Jaradat, P. D. Brimicombe, C. Southern, S. D. Siemianowski, E. DiMasi, M. Osipov, R. Pindak, and H. F. Gleeson, Phys. Rev. E **77**, 010701 (2008).

[27] S. Jaradat, P. D. Brimicombe, M. A. Osipov, R. Pindak and H. F. Gleeson, App. Phys. Lett. **98**, 043501 (2011).

[28] H. F. Gleeson, S. Jaradat, A. Labeeb and M. Osipov, Ferroelectrics, **431**, 40 (2012).

[29] A. Iida, I. Nishiyama, and Y. Takanishi, Phys. Rev. E **89**, 032503 (2014).

[30] A. Iida, Y. Takanishi, A. Fukuda, and J. K. Vij, Phys. Rev. E **94**, 052703 (2016)

[31] H. S. Chang, S. Jaradat, H. F. Gleeson, I. Dierking, and M. A.Osipov, Phys. Rev. E **79**, 061706 (2009).

[32] L. Johnson, S. Jaradat, and H. F. Gleeson, J. Mater. Chem. C **2**, 147 (2014)

[33] A.-M. Levelut and B. Pansu, Phys. Rev. E **60**, 6803 (1999).

[34] M. A. Osipov and M. V. Gorkunov, Liq. Cryst. **33**, 1133 (2006).

[35] A. D. L. Chandani, A. Fukuda, J. K. Vij, Y. Takanishi, and A. Iida, Phys. Rev. E **93**, 042707 (2016).

[36] A. V. Emelyanenko, Ferroelectrics, **495**, 129 (2016).

[37] A. D. L. Chandani Perera, A. Fukuda, J. K. Vij, and Y. Takanishi, Liq. Cryst., **44**, 1787 (2017).

Figure Captions

Fig. 1 Molecular structures of samples AS620 and AS657.

Fig. 2 Series of resonant X-ray scattering (RXS) profiles obtained at applied voltages from ±45.0 V to ±52.0 V at 86.3 °C. In (c) and (d), dotted lines indicate magnified profiles. Open circles in (c) and filled circles in (d) indicate positions where reflection peaks owing to C_{9p} and C_{6p} configurations, respectively, are expected to appear. Inset in (a) shows a two-dimensional diffraction pattern from which the one-dimensional RXS profile was extracted. White circle (B.S.) corresponds to the shadow of the direct beam stopper, the strong arc-like spot on the right (Bragg) is the first-order Bragg diffraction peak, and two weak RXS reflections (arrows) are seen between "B.S." and "Bragg". cps: counts/s.

Fig. 3 Sample photographs at applied voltages of (a) ±45.6 V and (b) ±54.5 V at 86.3 °C. The layer normal was approximately horizontal. Black arrows in (a) show phase boundary between three-layer and nine-layer periodic phases. In photo (b), most of the field of view is transformed to the SmC^* phase. In (b), the white arrow indicates a typical measurement point, and the black scale bar represents 0.1 mm. Blot-like patterns of various sizes and shapes are due to contamination on the outside of the glass plates.

Fig. 4 Series of RXS profiles obtained at applied voltages of ±14.0 V to ±40.0 V at 88.0 °C. In (d), (e), and (g), dotted lines indicate magnified profiles. Asterisks in (d), open circles in (e), and

filled circles in (g) indicate positions where reflection peaks resulting from C_{12p}, C_{9p}, and C_{6p} configurations, respectively, are expected to appear.

Fig. 5 Sample photographs at applied voltages of (a) ±0.0 V, (b) ±21.5 V, (c) ±30.8 V, and (d) ±33.7 V at 88.0 °C. In (d), the white arrow indicates typical measurement point, and the black scale bar represents 0.1 mm.

Table 1. Possible nine-layer Ising molecular configurations and corresponding squares of the relative structure factor for satellite reflections from 1/9 to 8/9. {· · · } represents the molecular configuration in a unit cell, and "R" and "L" indicate the smectic layer with directors tilted to the right and left, respectively. q_E numbers for each configuration are also shown in parentheses for reference.

	Satellites	Squares of the relative structure factor			
No.	Configurations (q_E)	1 (8) / 9	2 (7) / 9	3 (6) / 9	4 (5) / 9
1	RRRRRRRRL (7/9)	4.0	4.0	4.0	4.0
2	RRRRRRRLL (5/9)	14	9.4	4.0	0.5
3	RRRRRRLRL (5/9)	9.4	0.5	4.0	14
4	RRRRLRRRL (5/9)	0.5	14	4.0	9.4
5	RRRRRLRRL (5/9)	4.0	4.0	16	4.0
6	RRRRRRLLL (1/3)	26	7. 3	0	3.1
7	RRRRRLRLL (1/3)	16	1.9	12	6.6
8	RRRRLRRLL (1/3)	6.6	16	12	1.9
9	RRRRLRLRL (1/3)	7. 3	3.1	0	26
10	RRRLRRRLL (1/3)	3.1	26	0	7. 3
11	RRRLRRLRL (1/3)	1.9	6.6	12	16
12	RRRRRLLLL (1/9)	33	1.1	4.0	1.7
13	RRRRLRLLL (1/9)	20	5.9	4.0	11
14	RRRRLLRLL (1/9)	14	9.4	16	0.5
15	RRRLRRLLL (1/9)	11	20	4.0	5.9
16	RRRLRLRLL (1/9)	5.9	11	4.0	20
17	RRRLRLLRL (1/9)	9.4	5	16	14
18	RRRLLRRLL (1/9)	1.7	33	4.0	1.1
19	RRLRRLRLL (1/9)	4.0	4.0	28	4.0
20	RRLRLRRLL (1/9)	0.5	14	16	9.4
21	RRLRLRLRL (1/9)	1.1	1.7	4	33

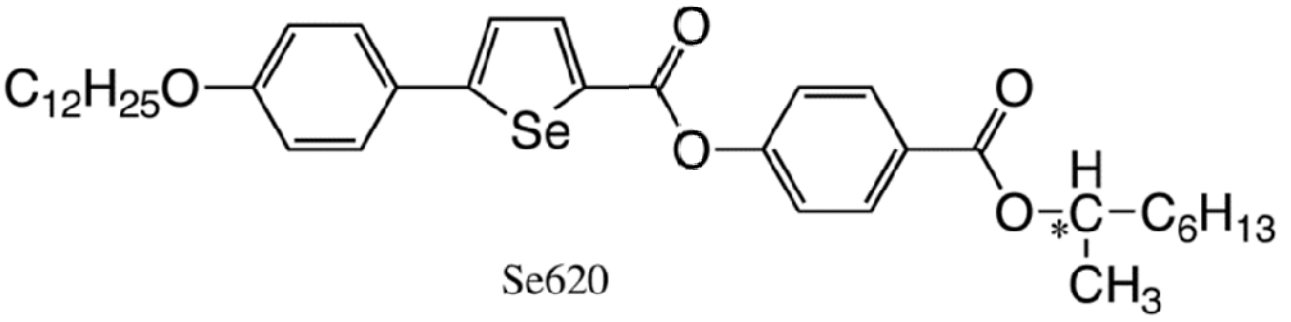

Se620

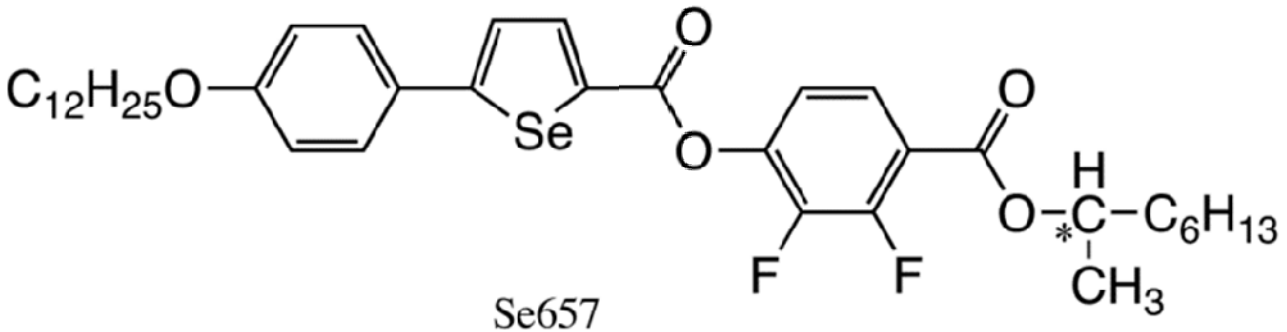

Se657

Fig.1

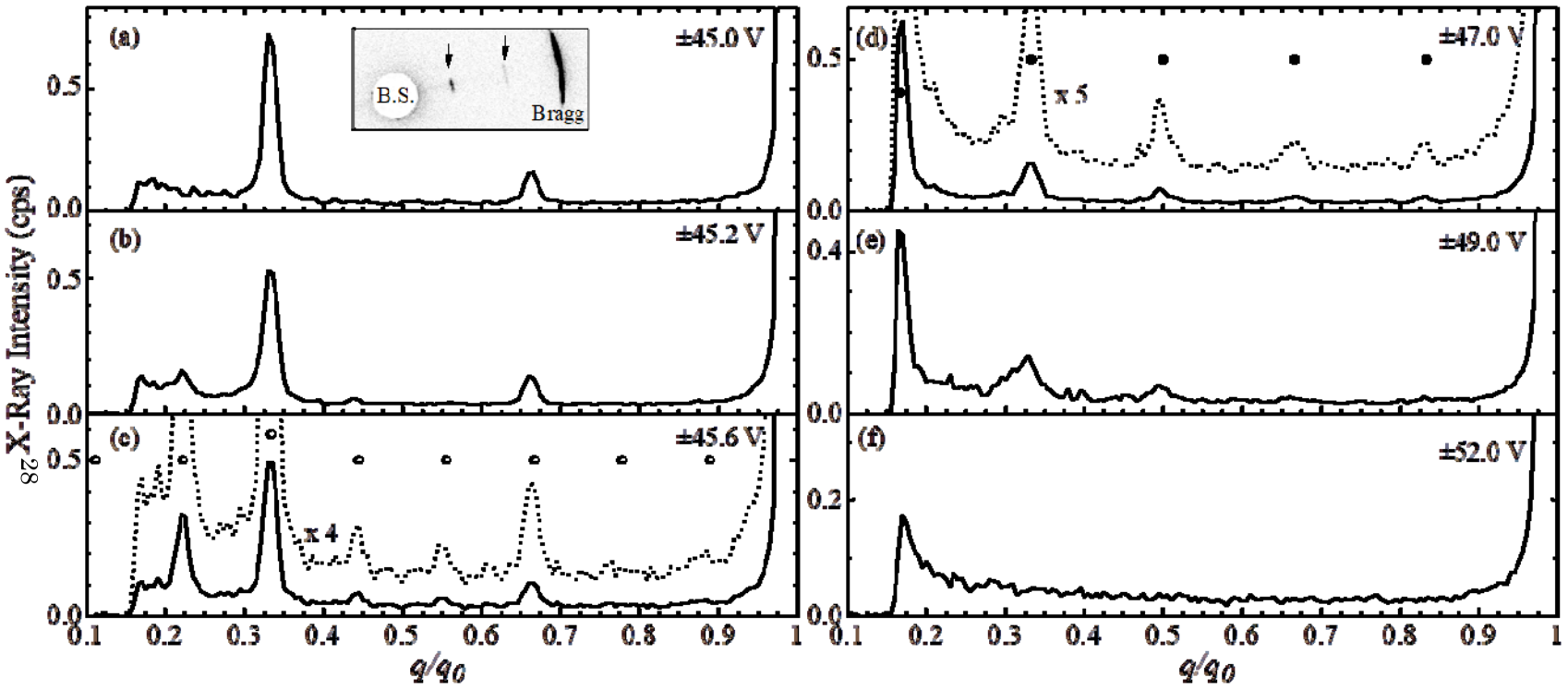
(a)
±45.0 V
B.S.
Bragg
(b)
±45.2 V
(c)
±45.6 V
x 4
(d)
±47.0 V
x 5
(e)
±49.0 V
(f)
±52.0 V
X-Ray Intensity (cps)
q/q0
q/q0

Fig.2

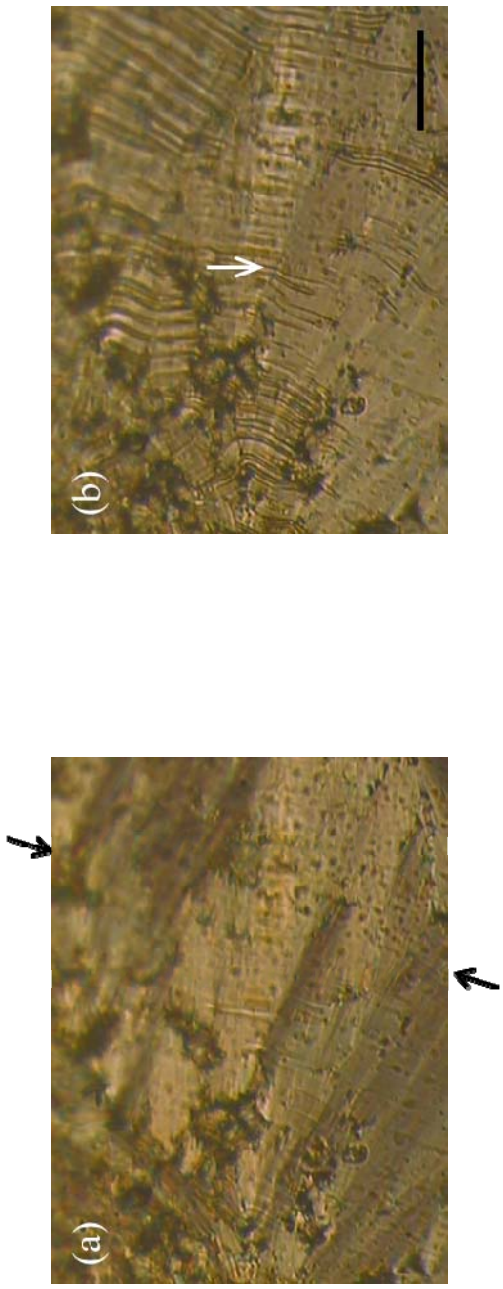

Fig.3

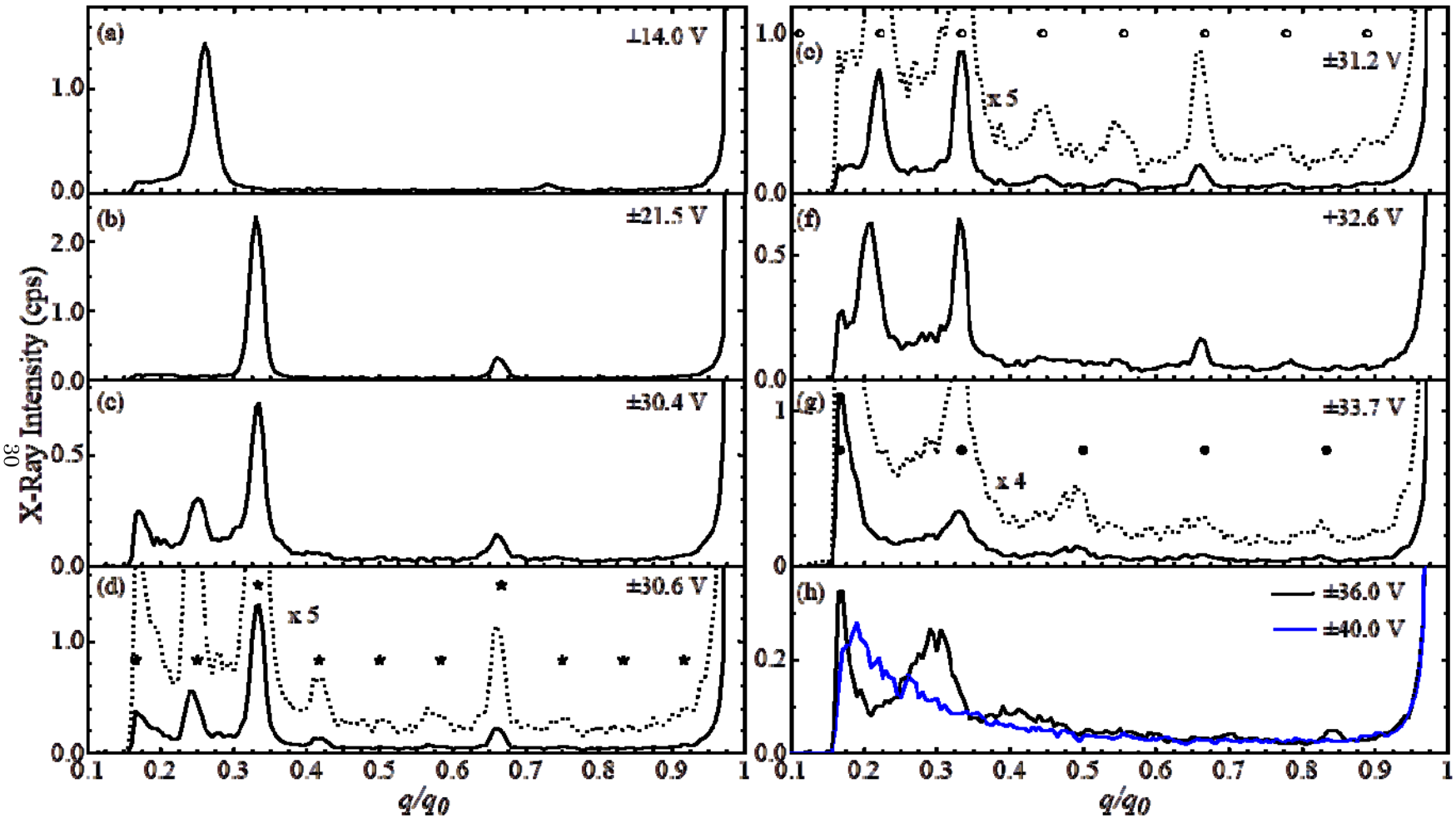
(a)
±14.0 V
(b)
±21.5 V
(c)
±30.4 V
(d)
±30.6 V
x 5
(e)
±31.2 V
x 5
(f)
+32.6 V
(g)
±33.7 V
x 4
(h)
±36.0 V
±40.0 V
X-Ray Intensity (cps)
q/q0
q/q0

Fig.4

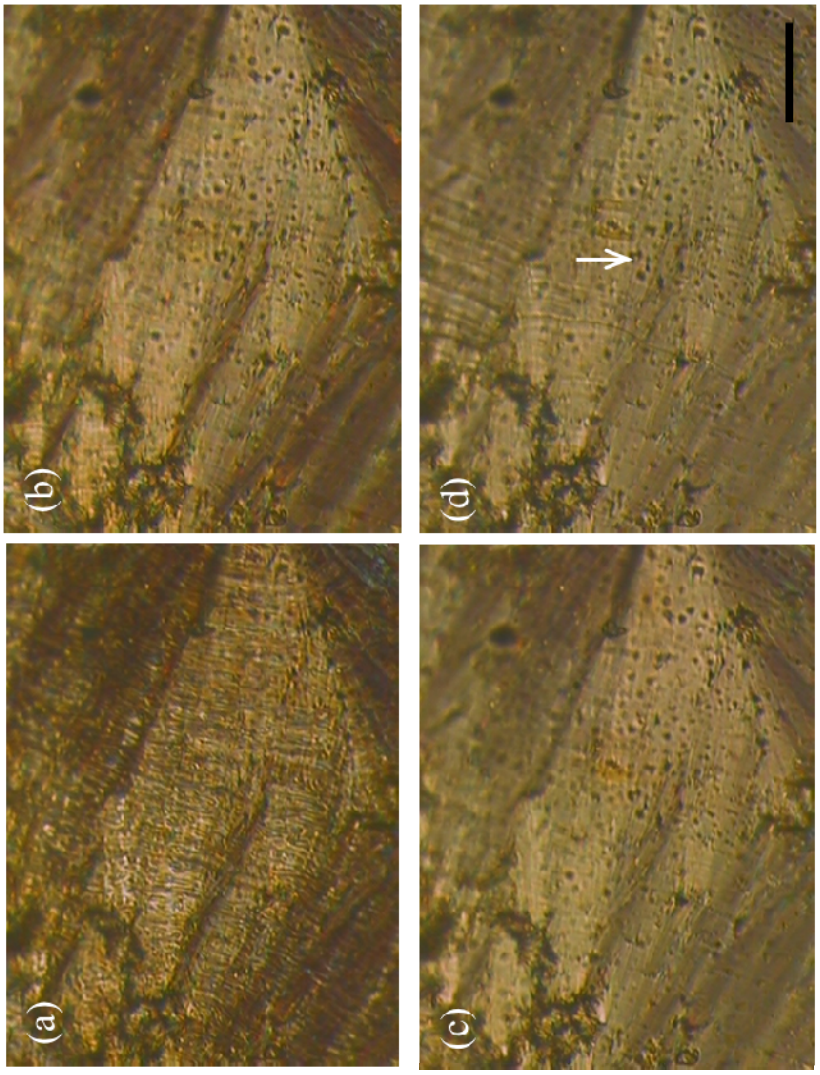

Fig.5